Microstructure and mechanical properties of Fe–Si–Ti–(Cu, Al) heterostructured ultrafine composites

J.M. Park [a,b,*], D.H. Kim [b], N. Mattern [a], K.B. Kim [c], E. Fleury [d], J. Eckert [a,e]

[a] IFW Dresden, Institute for Complex Materials, Helmholtzstr. 20, P.O. Box 27 01 16, D-01171 Dresden, Germany
[b] Center for Non-Crystalline Materials, Department of Metallurgical Engineering, Yonsei University, 134 Shinchon-dong Seodaemun-gu, Seoul 120-749, Republic of Korea
[c] Department of Advanced Materials Engineering, Sejong University, 98 Gunja-dong, Gwnagjin-gu, Seoul 143-747, Republic of Korea
[d] Advanced Metal Research, Korea Institute of Science and Technology, Seoul 130-650, Korea
[e] TU Dresden, Institute of Materials Science, D-01062 Dresden, Germany

ARTICLE INFO

ABSTRACT

The influence of partial substitution of Fe by Cu or Al in $Fe_{75-x}Si_{15}Ti_{10}(Cu, Al)_x$ ($x=0$ and 4) ultrafine composites on the microstructure and mechanical properties has been investigated. The $Fe_{71}Si_{15}Ti_{10}Cu_4$ ultrafine composite exhibits a favorable microstructural evolution and improved mechanical properties, i.e., large plastic strain of ~5% and pronounced work hardening characteristics. The mechanical properties of the ultrafine eutectic composite are strongly linked to the length scale heterogeneity and the distribution of the constituent phases.

© 2010 Elsevier B.V. All rights reserved.

1. Introduction

In situ bulk nanostructure-dendrite composites consisting of micron-scale dendrites and nano-scale eutectic matrix have become important as one of the novel ways to obtain high strength and plasticity at room temperature [1–3]. For example, Ti-based nanostructure-dendrite composites containing Nb and Ta acting as stabilizers for the micron-scale dendritic β-solid solution phases present a high strength of ~2.5 GPa together with a plastic strain of ~20% upon room temperature compression [4]. Detailed investigations on the deformation-induced microstructural changes of such high strength ductile Ti-based nanostructure-dendrite composites revealed a homogeneous distribution of slip bands in the micron-scale dendrites at the early stage of deformation [5–7]. With further compression, there is a pronounced interaction between shear and slip bands accompanying local structural transformations [8,9]. At the same time, the nanometer-scale eutectic matrix is overall rearranged along the direction of the primary shear bands hindering the propagation of secondary shear bands by forming a sandwich-like microstructure [5,10,11]. In this scenario, it is suggested that the eutectic matrix with nano- or ultrafine scale plays an important role to control the macroscopic plasticity besides the influence of the micrometer-scale dendrites.

Recently, ductile bimodal ultrafine eutectic composites without additional micrometer-size toughening phase have been developed [12–15]. In this case, the length scale heterogeneity of the eutectic phase contributes to the plasticity enhancement in such high strength nano-/ultrafine eutectic composites [16–19]. These recent investigations suggest that the combination of refining the lamellar spacing and obtaining a favorable distribution of a bimodal eutectic microstructure represents an effective route to develop a new class of advanced metallic materials with enhanced mechanical properties.

In this study, novel heterostructured ultrafine composites with improved mechanical properties have been developed in Fe–Si–Ti–(Cu, Al) alloys by combining the appropriate selection of additional elements concerning the solubility between the main constituent element (Fe) with the relatively high cooling rate of copper mold casting [20]. We demonstrate the role of additional elements on the microstructural evolution and the mechanical properties. The governing factors to control the plasticity of the ultrafine eutectic composites will be discussed.

2. Experimental

The $Fe_{75-x}Si_{15}Ti_{10}(Cu, Al)_x$ ($x=0$ and 4) alloys were prepared by arc melting of the high purity elemental constituents (99.99 wt.%) under an argon atmosphere followed by copper mold casting into cylindrical cavities with a diameter of 2 mm diameter and a length of 50 mm. Microstructural analysis of the as-cast and

* Corresponding author at: IFW Dresden, Institute for Complex Materials, Helmholtzstr.20, P.O. Box 27 01 16, D-01171, Dresden, Germany. Tel.: +49 351 4659 878.
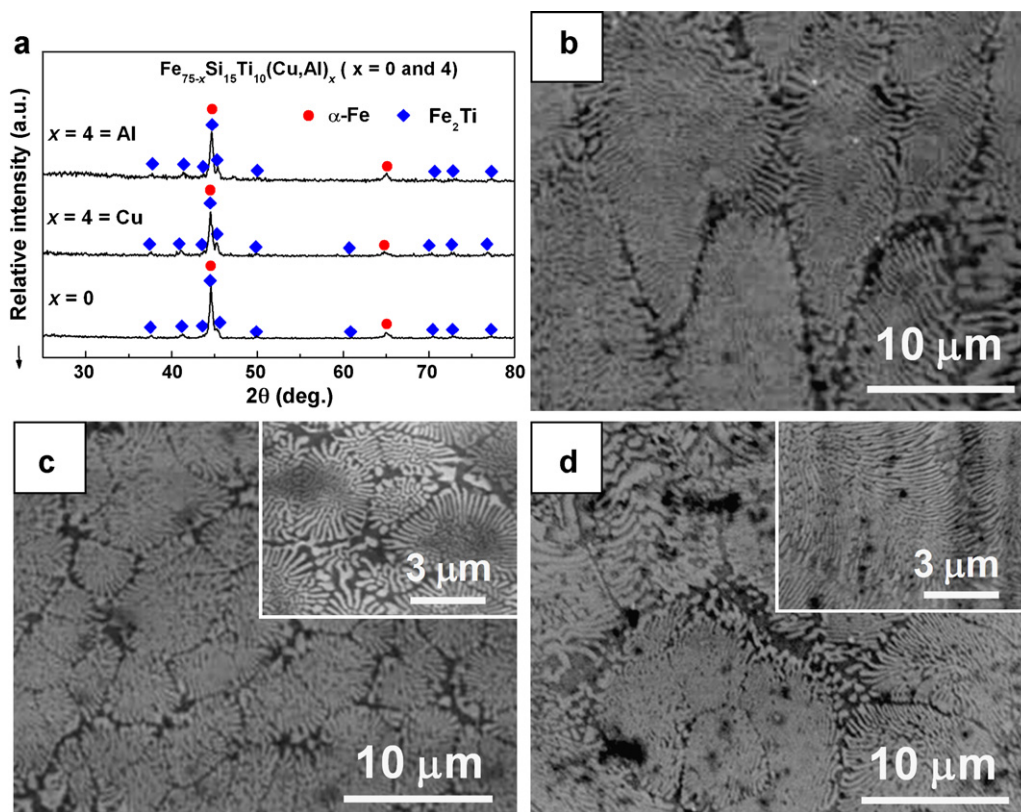*E-mail addresses:* j.m.park@ifw-dresden.de, jinman_park@hotmail.com (J.M. Park).

Fig. 1. XRD patterns (a) and SEM secondary electron images (b)–(d) of the as-cast $Fe_{75-x}Si_{15}Ti_{10}(Cu, Al)_x$ alloys with $x = 0$ and 4.

deformed samples was performed by scanning electron microscopy (SEM; Hitachi S-2700). Transmission electron microscopy (TEM; JEM 2100F) coupled with energy dispersive X-ray spectrometry (EDX; Oxford instrument INCA system) and X-ray diffraction (XRD; Rigaku CN2301, monochromatic Cu K_α radiation) experiments were used for phase and structure characterization. Thin foils for TEM investigation were prepared by conventional ion milling (PIPS; Gatan Model 600). In order to evaluate the mechanical properties in compression, cylindrical specimens with an aspect ratio of 2:1 were prepared and tested at room temperature under quasistatic loading using an initial strain rate of $1 \times 10^{-4}\,s^{-1}$.

3. Results and discussion

Fig. 1 shows the XRD patterns (a) and the secondary electron SEM images (b)–(d) of the as-cast $Fe_{75-x}Si_{15}Ti_{10}(Cu, Al)_x$ ($x = 0$ and 4) alloys. For all samples, the XRD patterns (Fig. 1(a)) reveal more or less the same diffraction peaks. The XRD diffraction peaks are identified as a mixture of α-(Fe, Si) solid solution ($Im\bar{3}m$, $a = 0.2857\,nm$) and (Fe, Si)$_2$Ti Laves phases ($P6_3$/mmc, $a = 0.4761\,nm$ and $c = 0.7755\,nm$). The lattice parameters of the α-(Fe, Si) solid solution and the (Fe, Si)$_2$Ti phases are considerably smaller than those of pure α-Fe ($Im\bar{3}m$, $a = 0.28664\,nm$) and equiatomic Fe$_2$Ti ($P6_3$/mmc, $a = 0.4785\,nm$ and $c = 0.7799\,nm$) [21] due to the dissolution of Si in α-Fe and Fe$_2$Ti, respectively. Figs. 1(b)–(d) depict SEM images of the as-cast $Fe_{75-x}Si_{15}Ti_{10}(Cu, Al)_x$ ($x = 0$ and 4) alloys. The microstructure of all samples exhibits a cellular eutectic morphology with a lamellar structure within the cells. The size of the eutectic cells is a few micrometers in length and the lamellar spacing in the cell interior is finer than that between the neighboring cells. For the $Fe_{75}Si_{15}Ti_{10}$ alloy (Fig. 1(b)), the microstructure over the cross-sectional area exhibits directional growth of eutectic cells along the radial direction. The majority of the lamellae within the cells are well aligned. The size of the eutectic cells is ~30 μm in length and ~10 μm in width, yielding an aspect ratio of ~3. The average lamellar thickness inside the cells is about 250–400 nm. In case of the Cu-containing alloy, the eutectic cells

are somewhat finer (~5 μm) and have a more pronounced spherical shape compared to the Cu-free alloy, but the average lamellar spacing ($300 \pm 100\,nm$) is not markedly different. The Al-bearing alloy (Fig. 1(d)) displays a similar shape of the eutectic cells with pronounced spherical morphology. However, the size and distribution of the eutectic cells is quite different. The size of the colonies is much bigger than that in Fig. 1(c). In addition, the lamellar thickness (100–200 nm) is slightly reduced and their distribution becomes more irregular and inhomogeneous.

In order to gain a deeper insight into the ultrafine eutectic microstructures, TEM investigations were performed. Figs. 2(a)–(c) shows bright-field (BF) TEM images and Figs. 2(d)–(g) selected area electron diffraction (SAED) patterns for the as-cast $Fe_{75-x}Si_{15}Ti_{10}(Cu, Al)_x$ ($x = 0$ and 4) alloys. The BF TEM images (Figs. 2(a)–(c)) show highly magnified alternating lamellae inside the cells, in agreement with Figs. 1(b)-(d). Figs. 2(d)–(e) obtained from the individual bright and dark contrast of the alternating lamellar layers of the $Fe_{75}Si_{15}Ti_{10}$ alloy were identified as the [1 0 0] zone axis of the hexagonal closed packed (hcp) (Fe, Si)$_2$Ti phase and the [1 1 0] zone axis of the body centered cubic (bcc) α-(Fe, Si) phase, respectively. Moreover, diffraction spots from both phases are observed by the [1 0 0] diffraction pattern of the hcp (Fe, Si)$_2$Ti phase and [1 1 0] zone of the bcc α-(Fe, Si) phase, as depicted in Fig. 2(f). EDX analysis reveals that the bright contrast phases contain more Ti ($Fe_{61.8}Si_{19.7}Ti_{18.7}$ for the $Fe_{75}Si_{15}Ti_{10}$ alloy, $Fe_{57}Si_{17.8}Ti_{24}Cu_{1.2}$ for the $Fe_{71}Si_{15}Ti_{10}Cu_4$ alloy and $Fe_{58.3}Si_{17.2}Ti_{23.1}Al_{1.4}$ for the $Fe_{71}Si_{15}Ti_{10}Al_4$ alloy), whereas the dark contrast phases are enriched in Fe ($Fe_{86.8}Si_{11.8}Ti_{1.4}$ for the $Fe_{75}Si_{15}Ti_{10}$ alloy, $Fe_{84.1}Si_{10.6}Ti_{1.5}Cu_{3.8}$ for the $Fe_{71}Si_{15}Ti_{10}Cu_4$ alloy and $Fe_{84.1}Si_{10.5}Ti_{1.6}Al_{3.8}$ for the $Fe_{71}Si_{15}Ti_{10}Al_4$ alloy) compared to the nominal alloy composition, respectively. Based on the results of phase, structure and chemical analyses, the ultrafine eutectic structure is composed of alternating lamellae of bcc α-(Fe, Si) and hcp (Fe, Si)$_2$Ti phases. In particular, for the Cu-bearing alloy,

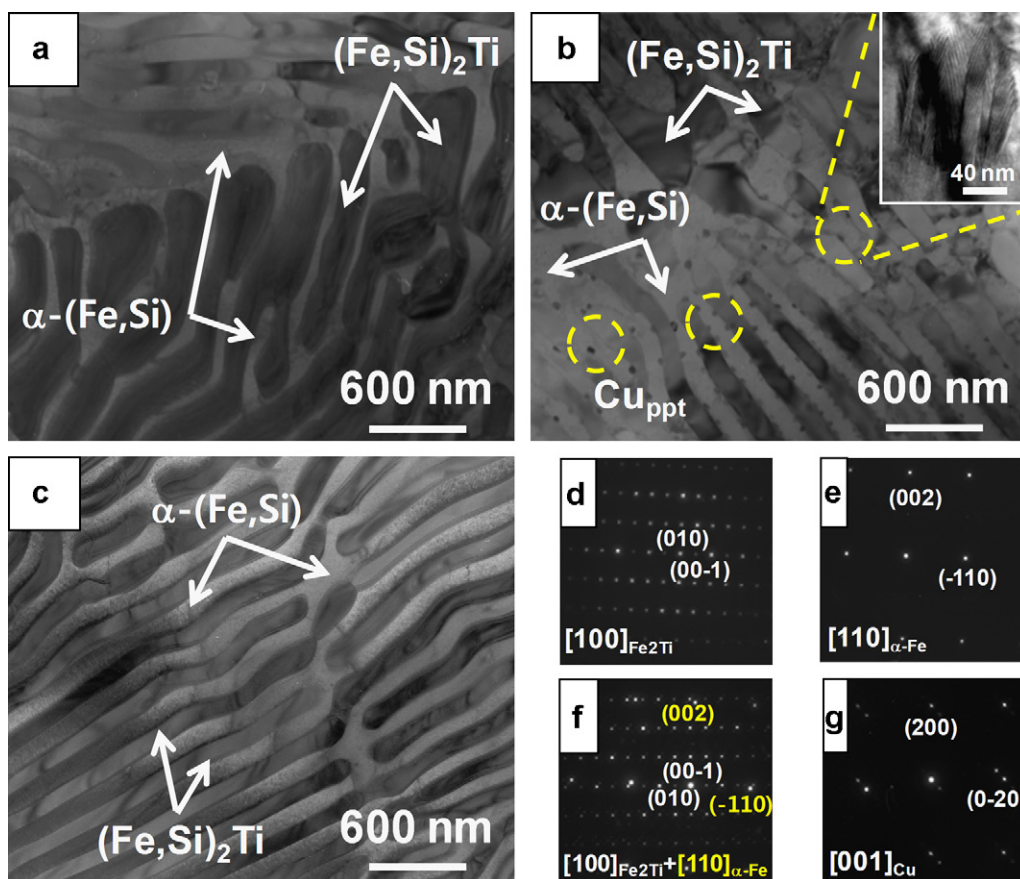**Fig. 2.** BF TEM images (a)–(c) and corresponding SAED patterns (d)–(g) for the as-cast $Fe_{75-x}Si_{15}Ti_{10}(Cu, Al)_x$ alloys with $x = 0$ and 4.

nano-scale spherical precipitates in the 5–50 nm size range are homogeneously distributed in the α-(Fe, Si) layers appearing with bright contrast. The interfaces between the individual lamellar layers are favorable precipitation sites that are presumably formed through partitioning of copper from α-(Fe, Si) and (Fe, Si)$_2$Ti with an excess of copper. The inset in Fig. 2(b) shows a highly magnified bright-field micrograph for the dotted circle region in Fig. 2(b). Moiré fringes within the precipitates are clearly observed. From the SAED patterns (Fig. 2(g)) and EDX analysis, the nano-scale precipitates within the α-(Fe, Si) phases were identified as a fcc-type Cu-rich phase (chemical composition: $Fe_{10.2}Si_{1.4}Ti_{0.7}Cu_{87.7}$).

From these results, one can suppose that the present specific microstructures form due to (i) the immiscibility between Fe and Cu and due to (ii) the large solubility between α-Fe and Al in the liquid state [20]. During solidification, long-range diffusion in front of the solid/liquid interface decreases and the destabilization of the regular eutectic morphology is accelerated simultaneously (see Figs. 1 and 2). In other words, novel heterostructured ultrafine composites can be tailored by adding additional elements (Al or Cu) with a high solubility or immiscibility in the major solvent species (Fe), resulting in a transformation of the eutectic growth behavior [22]. The significant difference in the solubility of the additional elements in α-Fe induces a morphological instability during the eutectic solidification, which is additionally influenced by the topological and crystallographic anisotropy of the two-phase solid/liquid interface [23]. A selective and inhomogeneous solute distribution most likely causes irregular eutectic growth, and thus the melt eventually solidifies into the specific spherical bimodal eutectic structures with ultrafine scale and an evident length-scale heterogeneity shown here. In particular, in case of the Cu-bearing alloy, nano-scale precipitation occurs during solidification due to an

excess of copper in the solid phase [24]. On the other hand, the addition of Al renders the eutectic growth more sluggish by increasing the liquid viscosity, favoring the refinement of the lamellar spacing [22,23].

Fig. 3(a) presents the room temperature engineering stress-strain curves of the as-cast $Fe_{75-x}Si_{15}Ti_{10}(Cu, Al)_x$ ($x = 0$ and 4) samples tested in compression. The values of the yield stress, σ_y, the ultimate compressive stress, σ_{max}, and the plastic strain, ε_p, for the as-cast samples are summarized in the inset in Fig. 3(a). All samples exhibit a high fracture strength of $\sim 3 \pm 0.2$ GPa, whereas the plasticity strongly depends on the additional element. For the Al-bearing alloy, the yield and fracture strengths are slightly increased from 2.8 GPa and 2.9 GPa to 3.1 GPa and 3.2 GPa, respectively. In contrast, the Cu-containing alloy shows an improved plasticity of $\sim 5\%$ (~ 10 times) as well as high strength. These results clearly show that the enhancement of the mechanical properties of heterostructured ultrafine composites is closely associated with the modulation of the eutectic structure including the length scale, the shape and the distribution of the phases in the microstructures, as shown in Figs. 1(b)–(d) and 2.

In order to understand the deformation behavior and mechanism of the heterostructured $Fe_{75}Si_{15}Ti_{10}Cu_4$ ultrafine composites with pronounced compressive plasticity, detailed investigations of a failed sample were performed by SEM (Fig. 3(b)). Two kinds of deformation bands are homogeneously distributed throughout the whole sample region, including localized sharp shear bands and a large amount of fine slip bands, as indicated by the dashed arrows and the squared region. The propagation of shear bands is inclined by about 45° to the direction of the applied load. As shown in the inset in Fig. 3(b), copious slip bands indicated by arrows without a preferred orientation with the stress axis are exten-
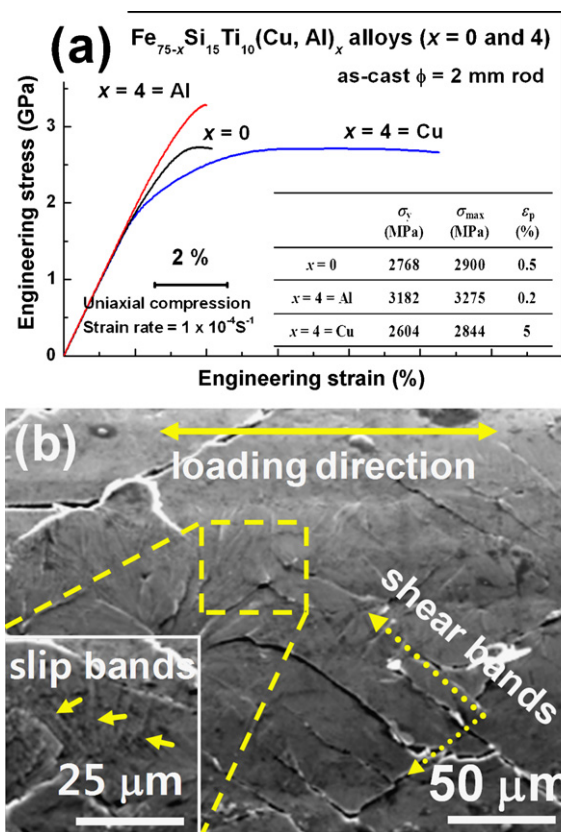
Fig. 3. (a) Room temperature compressive engineering stress–strain curves of the $Fe_{75-x}Si_{15}Ti_{10}(Cu,Al)_x$ rod samples with $x = 0$ and 4, and (b) a SEM secondary electron image of the lateral surface of the fractured $Fe_{71}Si_{15}Ti_{10}Cu_4$ sample: The inset shows the results of the compressive mechanical properties.

sively distributed on the surface of the failed sample. These findings reveal that the large plastic deformation of the heterostructured $Fe_{75}Si_{15}Ti_{10}Cu_4$ ultrafine eutectic composite is attributed to the pronounced dislocation activity. At the late stage of deformation, plastic deformation tends to be localized by formation of multiple shear bands, while dislocations still can be the carriers of plasticity in the shear band.

In the present investigation, the microstructure of all samples exhibits a bimodal-type eutectic morphology composed of nano-eutectic areas, which are encapsulated by sub-micron scale eutectic areas, revealing the length-scale heterogeneity of the lamellar structure. According to a recent report [14], these particular morphologies are proposed to be responsible for the enhanced macroscopic plasticity. It is suggested that the strong interaction between shear bands and the spatially heterogeneous structure can effectively avoid excessive shear localization, retard the plastic instability, and thus, endow uniform plastic deformation [15,16].

However, the $Fe_{75}Si_{15}Ti_{10}$ and $Fe_{71}Si_{15}Ti_{10}Al_4$ alloys in this study display very limited compressive plasticity compared to the $Fe_{71}Si_{15}Ti_{10}Cu_4$ alloy, although all these alloys have a bimodal eutectic structure. This result indicates that only the length-scale heterogeneity of an eutectic structure cannot be the governing factor to control the plasticity. Comparing the microstructures in more detail reveals that the eutectic cells of the Cu-bearing alloy are relatively finer ($\sim$5 μm) and have a more pronounced spherical shape. From the microstructural point of view, one can assume that fairly fine and spherical colonies allow for efficient dissipation of the shear stress and accommodation of excessive shear strain, caused by a rotation of the coarse eutectic areas against the fine eutectic areas acting as a pivoting point. Therefore, it is feasible to suggest that the specific ultrafine microstructure can effectively distribute

the localized shear deformation more homogeneously throughout the entire sample and multiple shear bands are generated, which in turn enhances the macroscopic plastic deformability.

As a consequence, a heterostructured $Fe_{71}Si_{15}Ti_{10}Cu_4$ ultrafine composite presents enhanced plasticity by creating a favorably modulated eutectic structure with length-scale heterogeneity, which does not need any other micrometer-size ductile dendritic phases to toughen the material.

4. Summary

Novel heterostructured ultrafine composites with enhanced mechanical properties were developed in the Fe–Si–Ti–(Cu, Al) system. By partial replacement of Fe by Cu or Al, the morphology of the eutectic colony becomes fine and more pronounced spherically. The microstructural changes are linked with a change of strength and plasticity. In particular, the $Fe_{71}Si_{15}Ti_{10}Cu_4$ ultrafine composite exhibits a high compressive strength of $\sim$2.7 GPa together with a distinct plasticity of $\sim$5%. The enhanced plasticity is ascribed to the homogeneous distribution of comparatively small and spherical eutectic colonies with bimodal length-scale lamellar spacing as well as the precipitation of nano-scale Cu in the α-(Fe, Si) phase. The rotational motion of spherical colonies can effectively dissipate localized shear stresses and accommodate complex plastic flow states. Accordingly, it is possible to tailor heterostructured ultrafine composite materials for desired properties by controlling the length-scale, the shape and the distribution of the phases in the bimodal eutectic structure.

References

[1] G. He, J. Eckert, W. Löser, L. Schultz, Nat. Mater. 2 (2003) 33.
[2] J.M. Park, S.W. Sohn, T.E. Kim, K.B. Kim, W.T. Kim, D.H. Kim, Scripta Mater. 57 (2007) 1153.
[3] D.V. Louzguine, L.V. Louzguina, H. Kato, A. Inoue, Acta Mater. 53 (2005) 2009.
[4] G. He, J. Eckert, W. Löser, Acta Mater. 51 (2003) 1621.
[5] K.B. Kim, J. Das, W. Xu, Z.F. Zhang, J. Eckert, Acta Mater. 54 (2006) 3701.
[6] B.B. Sun, M.L. Sui, Y.M. Wang, G. He, J. Eckert, E. Ma, Acta Mater. 54 (2006) 1349.
[7] D.V. Louzguine, H. Kato, L.V. Louzguina, A. Inoue, J. Mater. Res. 19 (2004) 3600.
[8] J. Das, J. Eckert, R. Theissmann, Appl. Phys. Lett. 89 (2006) 261907.
[9] D.V. Louzguine, L.V. Louzguina, V.I. Polkin, A. Inoue, Scripta Mater. 57 (2007) 445.
[10] J.M. Park, S.W. Sohn, T.E. Kim, D.H. Kim, K.B. Kim, W.T. Kim, J. Eckert, Appl. Phys. Lett. 92 (2008) 091910.
[11] L. Shi, H. Ma, T. Liu, J. Xu, E. Ma, J. Mater. Res. 21 (2006) 613.
[12] J.M. Park, J.H. Han, K.B. Kim, N. Mattern, J. Eckert, D.H. Kim, Philos. Mag. Lett. 89 (2009) 623.
[13] J. Das, K.B. Kim, F. Baier, W. Löser, J. Eckert, Appl. Phys. Lett. 87 (2005) 161907.
[14] J.M. Park, D.H. Kim, K.B. Kim, W.T. Kim, Appl. Phys. Lett. 91 (2007) 131907.
[15] L. Shi, J. Xu, E. Ma, Metall. Mater. Trans. A 39A (2008) 1225.
[16] J.M. Park, N. Mattern, U. Kühn, J. Eckert, K.B. Kim, W.T. Kim, K. Chattopadhyay, D.H. Kim, J. Mater. Res. 24 (2009) 2605.
[17] Z.Y. Suo, K.Q. Qiu, Q.F. Li, Y.L. Li, Y.L. Ren, Z.Q. Hu, J. Alloys Compd. 463 (2008) 564.
[18] L. Fu, J. Yang, Q. Bi, L. Li, W. Liu, J. Phys. D: Appl. Phys. 41 (2008) 235401.
[19] J.M. Park, K.B. Kim, D.H. Kim, N. Mattern, R. Li, G. Liu, J. Eckert, Intermetallics 18 (2010) 1829.
[20] H. Okamoto, Phase Diagrams for Binary Alloys, ASM International, Materials Park, OH, USA, 2000.
[21] JCPDFWIN, Version 2.2, JCPDS-International Center for Diffraction Data, 2001.
[22] M.C. Flemings, Solidification Processing, McGraw-Hill, New York, USA, 1974.
[23] R. Elliott, Eutectic Solidification Processing: Crystalline and Glassy Alloys, Butterworths, London, UK, 1983.
[24] H.K.D.H. Bhadeshia, R.W.K. Honeycombe, Steel: Microstructure and Properties, 3rd ed., Butterworth-Heinemann Press, Oxford, UK, 2006.